Applied Catalysis B: Environmental 320 (2023) 121972

Contents lists available at ScienceDirect

Applied Catalysis B: Environmental

journal homepage: www.elsevier.com/locate/apcatb

CO_2 methanation with Ru@MIL-101 nanoparticles fixated on silica nanofibrous veils as stand-alone structured catalytic carrier

Eva Loccufier [a,1], Geert Watson [b,1], Yingrui Zhao [c], Maria Meledina [d,e], Robbe Denis [a], Parviz Gohari Derakhshandeh [b], Pascal Van Der Voort [b], Karen Leus [b], Damien P. Debecker [c,*], Klaartje De Buysser [f], Karen De Clerck [a,*]

[a] Centre for Textile Science and Engineering (CTSE), Department of Materials, Textiles and Chemical Engineering, Ghent University, Technologiepark 70 A, 9052 Ghent, Belgium
[b] Centre for Ordered Materials, Organometallics and Catalysis (COMOC), Department of Chemistry, Ghent University, Krijgslaan 281-S3, 9000 Ghent, Belgium
[c] Institute of Condensed Matter and Nanoscience (IMCN), Université catholique de Louvain (UCLouvain), Place Louis Pasteur, 1, 1348 Louvain-La-Neuve, Belgium
[d] RWTH Aachen University, Central Facility for Electron Microscopy, D-52074 Aachen, Germany
[e] Forschungszentrum Jülich GmbH, Ernst Ruska-Centre (ER-C 2), D-52425 Jülich, Germany
[f] Sol-gel Centre for Research on Inorganic Powders and Thin Films Synthesis (SCRiPTS), Department of Chemistry, Ghent University, Krijgslaan 281 S3, 9000 Ghent, Belgium

ARTICLE INFO

Keywords:
Silica nanofibers
Metal-organic frameworks
Ruthenium nanoparticles
Heterogeneous catalysis
Structured catalyst

ABSTRACT

An important challenge in the valorization of CO_2 and H_2 into fuels is the development of a stable, reusable and easy to handle heterogeneous catalyst. Here, a silica nanofibrous membrane is investigated as carrier for Ru nanoparticles, themselves encapsulated inside the metal organic framework (MOF) Cr-MIL-101. The catalytic membrane is investigated for the Sabatier methanation reaction. The direct electrospinning of a tetraorthosilicate (TEOS) sol results in a highly thermal resistant silica nanofibrous structure (up to 1100 °C) with pores between the fibers in the μm-range, allowing a high gas throughput with low pressure requirements. A straightforward dip-coating procedure of the carrier was used to obtain a Ru@MIL-101 functionalized silica nanofibrous veil, avoiding Ru clustering. The obtained catalytic membrane exhibited an apparent turnover frequency of 3257 h^{-1} at 250 °C. This system therefore paves the way towards structured reactors for efficient CO_2 hydrogenation processes.

1. Introduction

Over the past decades, global awareness with respect to environmental pollution has significantly increased, resulting in a demand for tremendous action [1–3]. Reducing the net emissions of greenhouse gases, such as CO_2, is one of the crucial targets. A promising strategy is chemical conversion, since it is a straightforward way to reduce the emissions, and thus the concentration in the atmosphere [4–7]. There are already economically viable cases of "CO_2 Capture and Utilization" strategies (CCU), such as the production of urea, solvents (e.g. alcohols) and fuel gases, which clearly demonstrate the interest and relevance of chemical CO_2 conversion [8–14].

Among the various routes available, the hydrogenation of CO_2 to CH_4, also known as the Sabatier reaction, is one of the most challenging routes [15–18]. In general, CO_2 and H_2 are mixed (with a molar ratio of 1:4) under a high pressure and elevated temperatures over a metal-based hydrogenation catalyst, forming methane (CH_4) and water. In this way, an optimal balance between the temperature required to break the strong CO_2 bonds (thus overcoming the otherwise very slow kinetics), and the exothermic reaction limiting the CO_2 conversion (due to unfavorable thermodynamics at high temperatures) can be achieved. For this, Ru, Ni, Fe, Co, Pt nanoparticles immobilized on a support material, such as Al_2O_3, SiO_2 and TiO_2 are often used [12,19–31]. Among these various metals, Ru is one of the most promising catalysts in terms of oxygen binding energy [32–36]. However, as the reaction is known to be structure sensitive, effects such as sintering should be avoided, allowing the maintenance of a high dispersion of small Ru nanoparticles during reaction [35,37].

* Corresponding authors.
E-mail addresses: Damien.Debecker@UCLouvain.be (D. P. Debecker), Karen.Declerck@ugent.be (K. De Clerck).
[1] Authors contributed equally.

https://doi.org/10.1016/j.apcatb.2022.121972
Received 4 July 2022; Received in revised form 5 September 2022; Accepted 9 September 2022
Available online 16 September 2022

Metal organic frameworks (MOFs) are excellent candidates for applications in for example gas storage [38–42], separation [43–46], and heterogeneous catalysis [47–49] because of their very large surface areas (up to 4500 $m^2 g^{-1}$), tunable pore size and pore volume. The use of MOFs as support to encapsulate Ru nanoparticles in the pores can provide the required long-term stability of the catalyst [50,51]. A schematic presentation of the aimed at ideal encapsulation of Ru in a MIL-101 Cr-based MOF is given in Fig. 1, right.

Even though the encapsulation of Ru nanoparticles in a MOF structure tremendously increases their stability against clustering, the direct use of the small MOF crystals loaded with Ru nanoparticles cannot be envisaged on an industrial level. Therefore, shaping procedures should be applied, such as the compression into pellets to form shaped catalyst bodies which can be easily manipulated and which do not provoke excessive pressure drops in continuous reactors [52,53]. This, however, results in a significant decrease of the available surface area of the nanoparticles, and could lead to diffusional limitations in the catalyst bodies [54,55]. As an alternative, the catalyst particles can be deposited onto porous, easy-to-handle, and reusable structured supports [56–59].

The use of membrane structures for the process intensification of heterogeneous catalysis is very promising. In the first place for (waste) water purification [60–62], but nowadays, the use of membranes in catalytic reactors is also under intensive investigation [63–72]. The membrane can act as separation barrier, catalyst or a combination of both [13,23,73–75]. Electrospun nanofibrous membranes are ideal candidates, due to their highly porous structures (porosity > 80%) and large surface-to-volume ratio, allowing a high flux through the membrane [76–78]. In most cases, advanced polymers (e.g. PVDF, PEEK) are used because they allow a straightforward production process and have a relatively high thermal (max. 300–350 °C) and chemical resistance. However, high amounts of toxic solvents are often required to manufacture these membrane structures [13,79,80].

Today, the best combination of structural integrity, and thermal and chemical resistance is obtained by the use of inorganic alternatives [74, 81,82]. This results in a catalytic support withstanding extreme conditions [68,83–85]. To ensure a good mechanical stability, direct electrospinning of a ceramic network is preferred, leading to dense, continuous and flexible fibers. Nevertheless, most studies make use of a well-spinnable organic polymer which is added to the electrospin solution to promote the nanofiber production, after which a post calcination treatment is applied to obtain an inorganic nanofibrous veil [86–88]. This leads to an inherent reduction in sample robustness, and thus brittle nanofibrous veils which are less suitable as stand-alone structures.

In this work, we use the direct electrospinning of a sol-gel solution of a tetraethyl orthosilicate (TEOS) precursor to prepare flexible silica nanofibrous veils which exhibit a thermal resistance up to 1100 °C and show an outstanding stability in acidic environments [89–92]. The silica nanofibrous membranes were used as support for MOF-encapsulated Ru nanoparticles, see Fig. 1. More specifically, the Cr-based MOF, denoted as MIL-101, was used to embed the Ru particles because of its high thermal and chemical stability [93,94]. Moreover, the success of this encapsulation has been showcased before [50,51]. As a proof of concept, the resulting materials were evaluated in the Sabatier reaction using a layer construction of the catalytic structure inside a tubular reactor, see Fig. 1 left. It is demonstrated that a (silica) nanofibrous membrane is an excellent catalytic carrier material, and therefore paves the way towards membrane reactors and research into process intensification of inorganic nanofibrous membranes as highly thermal and chemical resistant catalytic carrier in a broad range of applications.

2. Materials and methods

2.1. Materials

All chemicals were purchased from TCI Europe, Sigma-Aldrich or Fluorochem and applied without additional purification. For the electrospinning process, the silica precursor tetraethyl orthosilicate (TEOS, reagent grade 98%) and the catalyst (hydrochloric acid; HCl, 37%) were obtained from Sigma-Aldrich and used as received.

2.2. Synthesis of MIL-101

A hydrothermal synthesis approach was utilized in which a Teflon lined container was filled with 4 mmol terephthalic acid, 4 mmol of Cr $(NO_3)_3 0.9\ H_2O$ and 20 mL demineralized water. The mixture was stirred for 10 min and placed in an autoclave, which was heated to 210 °C over 2 h and held at this temperature for 8 h. After filtration of the solid, several washing steps were performed to purify the material. Firstly, the MOF was stirred in DMF for 24 h to remove any organic residues. Next, the powder was collected through filtration, and placed in 1 mol L^{-1} HCl for 12 h to remove any excess of Cr salts. Hereafter, the material was washed with water until neutral pH. The purified MIL-101 material was dried under vacuum at 110 °C overnight prior to use.

2.3. Encapsulation of Ru nanoparticles within MIL-101

The ruthenium precursor, $RuCl_3$, was introduced into the MIL-101 support material based on the procedure described by Fang et al. [95]. A solution of 287 mg $RuCl_3$ in 56 mL acetone was added to a suspension of 700 mg MIL-101 in 14 mL acetone. The mixture was left to stir for 24 h after which the $RuCl_3$ @MIL-101 was collected through filtration.

In a following step, the ruthenium precursor was reduced using 9.3 mL of a 0.486 mol L^{-1} $NaBH_4$ solution to form the ruthenium nanoparticles. This solution was added dropwise to an aqueous dispersion of 700 mg $RuCl_3$ @MIL-101 in 23.3 mL of demineralized water, after which it was left to stir for 35 min at room temperature. Finally, the resulting encapsulated structure denoted as Ru@MIL-101 was collected through filtration and was washed with demineralized water, ethanol and acetone.

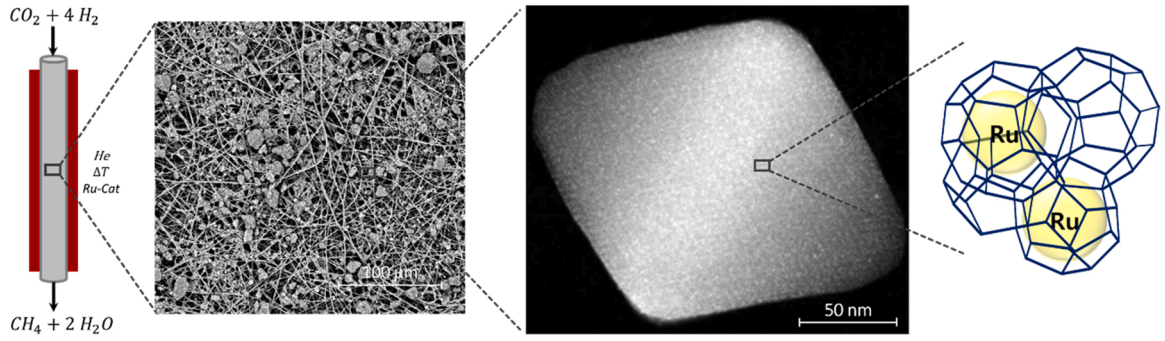

Fig. 1. Scheme of the incorporation of silica nanofibrous veils as support for MIL-101 nanostructures loaded with Ru nanoparticles to catalyze the hydrogenation of CO_2 to CH_4, also known as the Sabatier reaction. In this way, an easy-to-handle, macroscopic heterogeneous catalyst is created.

2.4. Electrospinning of TEOS-based nanofibers for membrane production

Silica nanofibers were made according to a methodology that combines electrospinning with sol-gel chemistry, as described in previous works [89,90,96]. Prior to electrospinning, the viscosity of the sol was measured using a Brookfield viscometer LVDV-II. The electrospinning experiments were executed on a rotating drum collector using a dual moving needle set-up (length of 50 cm and diameter of 12 cm). The tip-to-collector distance was fixed at 15 cm, with a flow rate of 1 mL h^{-1} and a voltage of 22 kV.

2.5. Attachment of catalytic nanoparticles on the electrospun silica nanofibrous veil

Both a pre- and a post-incorporation of the silica nanofibrous veils with Ru@MIL-101 nanoparticles was examined. Incorporation prior to electrospinning was achieved by mixing the Ru@MIL-101 nanoparticles in the sol on a stirring plate at room temperature. A mass ratio of the TEOS-based sol and the Ru@MIL-101 nanoparticles of 1:0.01 was used. Post-incorporation was performed via dip-coating of the pristine silica nanofibrous veils in a homogeneous Ru@MIL-101 suspension using a computer-controlled dip-coating unit from KSV Instruments in a clean room facility (class 100,000/1000). A mass concentration of 2.00 g Ru@MIL-101 particles L^{-1} in absolute ethanol resulted in a homogeneous suspension. Absolute ethanol as dip-coating solvent resulted in the highest long-term stability, enabling a stable dip-coating process. The samples were immersed for 2 min, removed at a speed of 170 mm min^{-1} and dried at room temperature for 24 h. The maximal coating speed of the equipment was used, leading to the highest particle loading as proven in previous research [97]. To increase the loading, varying the amount of coating cycles was investigated. A new coating was applied after complete drying of the previous coating.

Since it is possible to have a continuous production of electrospun nanofibrous membranes on an industrial scale, a direct dip-coating could can be incorporated in an up-scaled production line without a large increase in cost price, making this a competitive catalytic carrier material compared to other support materials described in literature [12,19–22,24–31].

2.6. Characterization of Ru@MIL-101@Silica nanofibrous veils

Nitrogen sorption analyses were performed on a Bel Japan Inc. Belsorp mini II instrument at 77 K. Prior to the N_2 sorption measurements, the samples were degassed at 120 °C under vacuum in order to remove any residual solvent molecules.

The Powder X-Ray Diffraction (XRD) measurements were performed on a Thermo Scientific ARL X'TRA Powder X-ray Diffractometer using Cu Kα radiation ($\lambda = 1.5406$ Å) at 40.00 kV and 30.00 mA under ambient conditions.

Annular dark field scanning transmission electron microscopy (ADF-STEM) and energy dispersive X-Ray (EDX) spectroscopy experiments were carried out using a FEI Titan transmission electron microscope operated at an accelerating voltage of 200 kV and equipped with a probe spherical aberration corrector unit and a Super-X EDX system [98]. The morphology and the diameters of the silica nanofibers and functionalized nanofibrous veils were examined using a Phenom Pharos Desktop Scanning Electron Microscope (SEM) at an accelerating voltage of 10 kV. Prior to analysis the samples were coated with a 15 nm coating using an automatic sputter coater (Plasmatool-SC Benelux Scientific, Au coating). Image J software was used to determine the nanofiber diameters by taking an average of 50 measurements.

Induced Coupled Plasma – Optical Emission Spectroscopy (ICP-OES) analysis was performed on a Varian Vista-MPXTM CCD instrument. Prior to analysis, the samples were dissolved using a 15.8 mol L^{-1} HNO_3 solution at 110 °C.

Hydrogen adsorption experiments were performed using a Quantachrome Autosorb-iQ instrument. The sample was first activated under constant helium gas flow at 120 °C, after which it was exposed to the analysis gas (H_2) until saturation. It was then evacuated at 120 °C to remove the physisorbed gas (reversible adsorption; residual pressure < 1 mbar). The remaining adsorbed gas was assigned to the adsorption corresponding to the H_2-chemisorption. An average of three measurements is reported, confirming a high reproducibility.

2.7. CO_2 methanation experiments

The metallic fixed-bed tubular reactor consists of a tube with a length of 15 cm and an inner diameter of 8 mm, and is surrounded by an isolating oven to control the temperature. The reactor was loaded with the Ru@MIL-101 nanoparticles, and Ru@MIL-101 @Silica nanofibrous veils to compare the catalytic activity. The powder was used as produced, and the nanofibrous veils were cut in small pieces and stacked in the reactor to allow use of the same reactor, with a total mass of respectively 15 and 100 mg. A mixture of CO_2 and H_2 was diluted with inert He gas to a molar ratio of 1:4:5 respectively. A total flow rate of 20 mL min^{-1} was used. All lines were heated to 120 °C to avoid any product condensation. The effluent gases go through an online gas chromatography setup (Varian CP3 800 with a Flame Ionization Detector and Thermal Conductivity Detector and Hayesep Q, Molsieve 5 A and CP-SIL-5CB columns) to measure the conversion of CO_2 and the production of CH_4. Stability tests were performed in the same reactor setup under the same conditions, simply altering the exposure time.

3. Results and discussion

3.1. Characterization of the Ru@MIL-101 material

The XRD patterns of the pristine MIL-101 and Ru encapsulated in MIL-101 material (denoted as Ru@MIL-101) are displayed in Fig. 2a. No change in the XRD pattern of the MIL-101 occurs upon the introduction of the Ru nanoparticles; in other words, the crystal structure of the framework remains intact. This was confirmed by means of Diffuse Reflectance Infrared Fourier Transform Spectroscopy (DRIFTS) measurements, as similar spectra were observed for both the Ru-loaded and pristine MIL-101 nanoparticles, see Fig. S1 in the Supporting Information.

Nitrogen adsorption analysis was performed to evaluate the porosity of both the pristine and the modified material, see Fig. 2b. The specific surface area (S_{BET}) of MIL-101 and Ru@MIL-101 are 2480 and 1600 m^2 g^{-1} respectively, whereas the pore volume of the pristine MOF support and Ru@MIL-101 material are 1.47 and 0.95 cm^3 g^{-1} respectively. Both decreases are a result of the encapsulation of Ru into the cages of the MIL-101 structure.

A combination of ADF-STEM imaging and EDX spectroscopy was applied to investigate the distribution of Ru within the MIL-101 framework. Fig. 3 depicts an ADF-STEM image and the corresponding EDX spectrum, showing a clear Ru signal. The bright contrast zones on the surface of the MIL-101 crystal corresponds to Ru-rich zones, of which a more detailed view is given in Fig. 4. Inside the hosting MIL-101 crystal heavier Ru particles are also showing up in a periodical manner (see evenly spread of red dots in Fig. 3b) – this could be seen as a fingerprint of filled pores. The indent of Fig. 4 shows that both the smaller and larger pores of the Cr-MIL-101 structure (as schematically depicted in Fig. 1) can be filled with Ru. An in-depth study of the encapsulation of Ru into MIL-101 MOF particles has been reported previously by Meledina et al. [50]. The same synthesis method has been used in this work.

Another important property of the catalytic powder is its thermal stability, since this determines the operation conditions of the reactor. Thermogravimetric analysis (TGA) of both the as-prepared MIL-101 and the Ru@MIL-101 framework show complete decomposition at 470 °C, with degradation starting from 350 °C onwards (see Fig. S2 in the

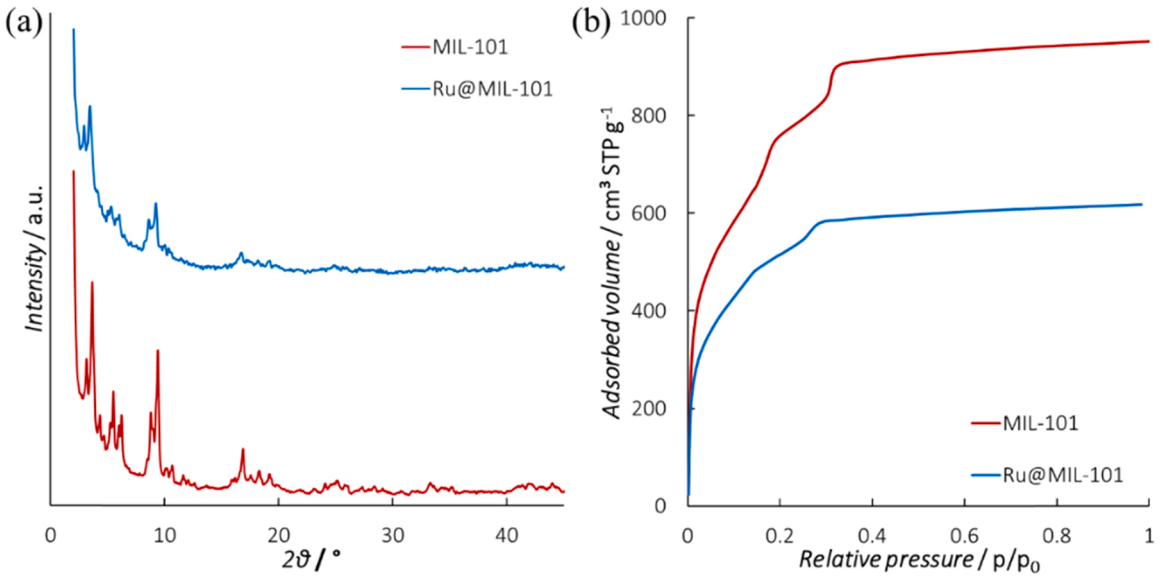

Fig. 2. (a) XRD patterns of the unmodified MIL-101 and the Ru@MIL-101 material. The diffraction pattern of MIL-101 is not affected by the incorporation of Ru nanoparticles. (b) Nitrogen adsorption isotherms of MIL-101 and Ru@MIL-101 showing a decrease in adsorbed volume due to the Ru encapsulation, resulting in a decreased specific surface area by approximately a third according to the BET model.

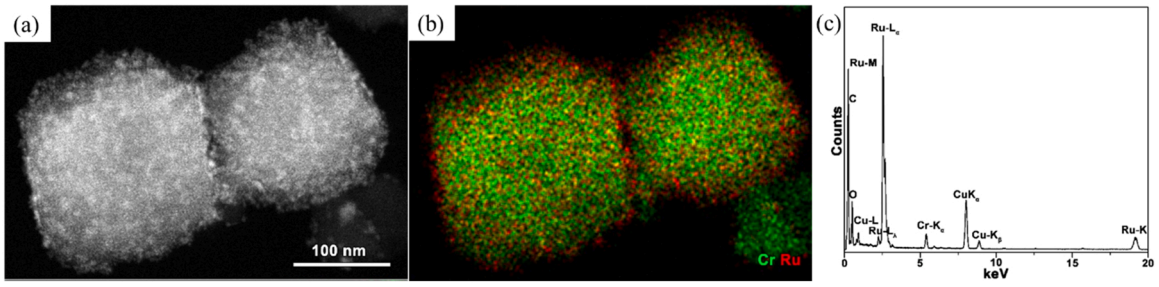

Fig. 3. (a) ADF-STEM image together with the corresponding (b) EDX map for Cr (green) and Ru (red). (c) EDX spectrum of Ru@MIL-101 nanoparticles.

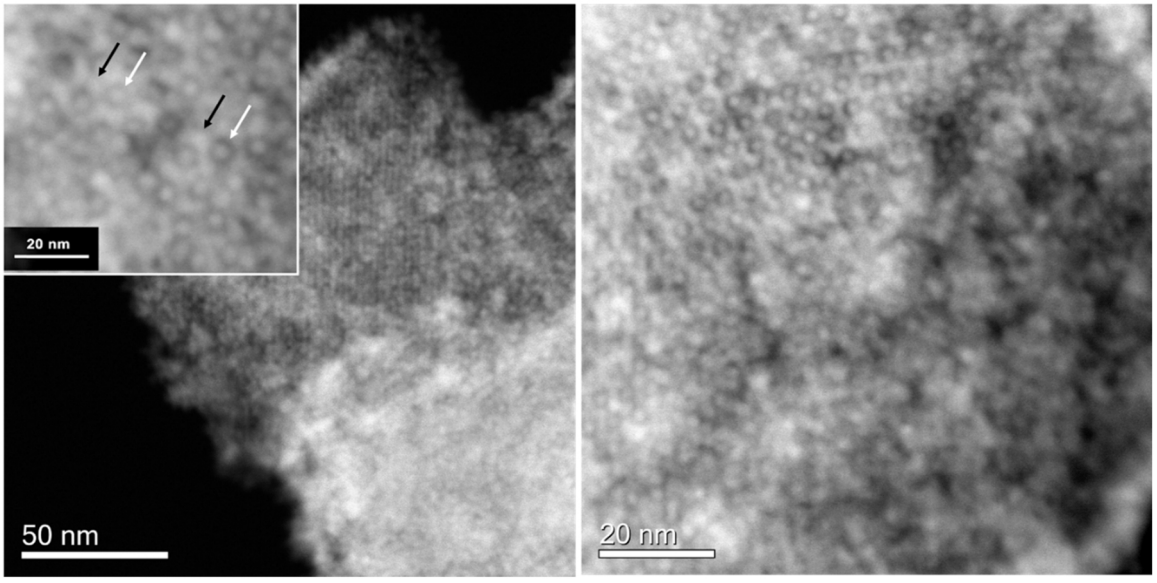

Fig. 4. HR ADF-STEM images of Ru@MIL-101 particles viewed along the [011] direction of MIL-101. The Ru appears brighter than the Cr-MIL-101 structure, showcasing a widespread filling of the both types of Cr-MIL-101 pores. In the indent, examples of both types are indicated using arrows. The larger pores of the Cr-MIL-101 cages are indicated with black arrows, and the smaller ones with white arrows.

Supporting Information). The thermal stability of the MIL-101 material is not altered upon the introduction of the Ru nanoparticles.

3.2. Silica nanofibrous veils as macroscopic and porous carrier of Ru@MIL-101

In a consecutive step, the Ru@MIL-101 particles were distributed onto the electrospun silica nanofibrous membranes to enhance the recyclability, avoid particle clustering during catalysis, and create a heterogeneous catalytic material on a macroscopic scale that is easy to manipulate, incorporate in reactor systems, and to recover and reuse. The carrier was created using both incorporation by mixing the particles with the sol prior to electrospinning, and post-incorporation of the as-spun silica membrane via a dip-coating technique.

A critical parameter to allow the incorporation of Ru@MIL-101 particles in the electrospin solution is the dynamic viscosity, and the alteration thereof upon mixing in of Ru@MIL-101 particles. In general, for TEOS-based sols, electrospinning is performed between 100 and 200 mPa s [90]. Addition of the catalytic particles is therefore limited to the range in which it does not alter the dynamic viscosity drastically. Otherwise, the fibers become too thick, or electrospinning is not possible anymore because the electric field cannot overcome the surface tension of the solution. Stable electrospinning was achieved upon the addition of 1 wt% Ru@MIL-101 particles (1 g particles/100 g sol) to the prepared sol at 0.9 mL h^{-1}, 21 kV and a needle-to-collector distance of 15 cm. Although this resulted in continuous fibers with a small diameter, the particles were completely encapsulated by the silica matrix. In addition, some thicker beads were formed, probably due to clustering of the Ru@MIL-101 particles in the sol (Fig. 5a). Furthermore, a higher loading of the sol resulted in a non-electrospinnable solution.

Dip-coating of the electrospun membrane in a solution with the dispersed nanoparticles was investigated as an alternative route. The prepared Ru@MIL-101 particles were dispersed in absolute ethanol using a concentration of 2 g L^{-1}. This resulted in a stable suspension for dip-coating. Lower Ru@MIL-101 concentration resulted in lower particle loading after coating, and higher mass concentrations resulted in less stable coating solutions. It was proven that the Ru@MIL-101 particles remain stable in absolute ethanol for at least one year, allowing long-term storage and usage as a dip-coat solution (see Fig. S3 in the Supporting Information). To account for the polarity of the solvent, super-hydrophilic silica nanofibrous veils were used, which were obtained after a thermal treatment at 500 °C for 1 h at atmospheric pressure in air [97]. The nanofibrous veils were immersed in the coating solution for 2 min, after which they were removed at a withdrawal speed of

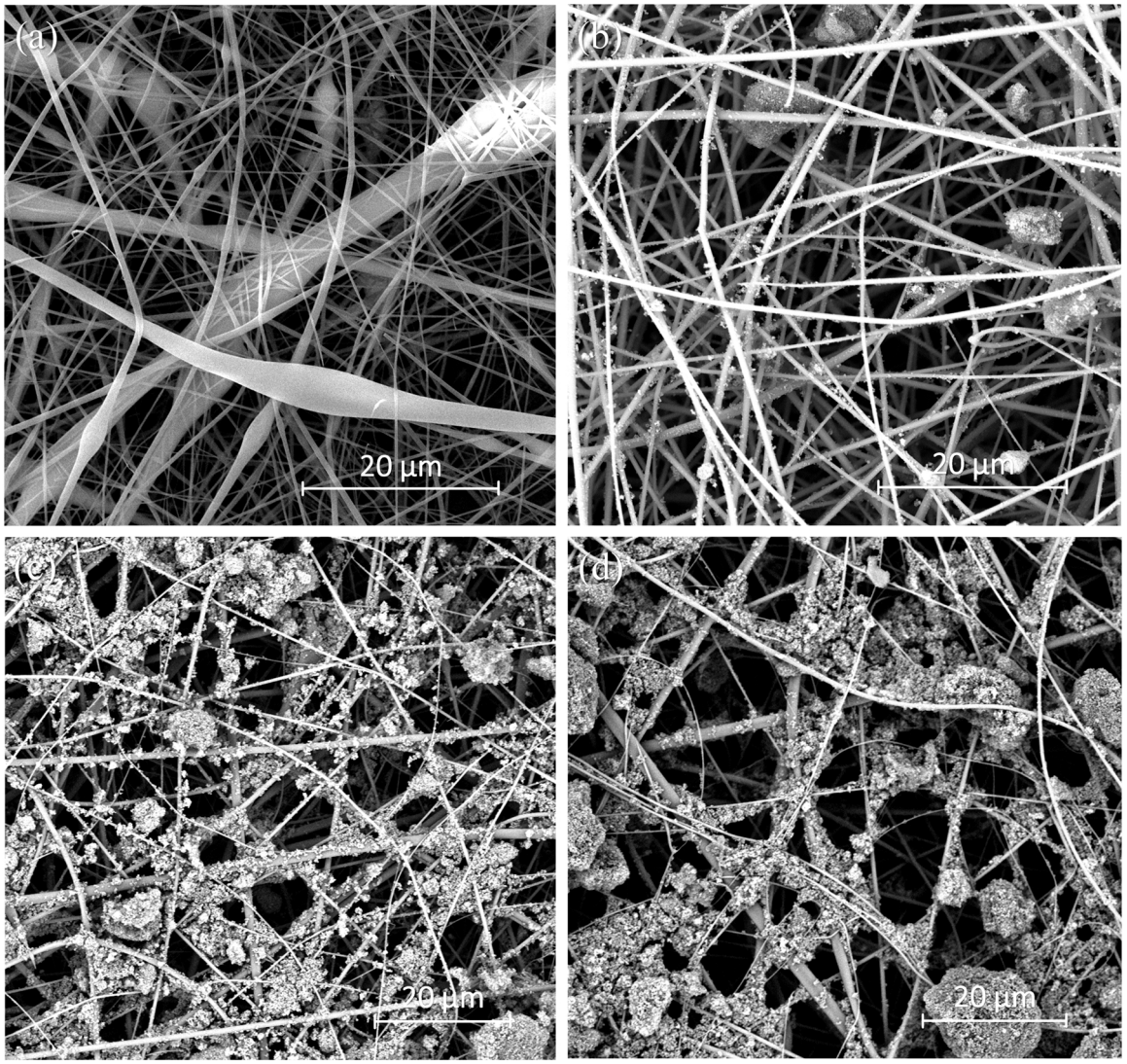

Fig. 5. SEM images of silica nanofibrous veils functionalized with Ru@MIL-101 nanoparticles using two different methods: (a) inline functionalization with 1 wt% in the sol prior to electrospinning, and post-functionalization via dip-coating in a 2 g L^{-1} dispersion in ethanol absolute at 170 mm min^{-1} for (b) 1 cycle, (c) 2 cycles and (d) 3 cycles. Dip-coating results in a good distribution of the particles, without significant loss in porosity of the nanofibrous veils.

170 mm min^{-1}. The resulting Ru@MIL-101 coatings showed a good distribution of the individual particles on the fibers, and only minor fractions of clusters were observed (Fig. 5b). To increase the overall loading, multiple coatings, using the same coating solution, were performed, with a drying step in between, see Fig. 5c-d. The quantitative amount of Ru present in the obtained membranes is presented in Table 1. Increasing the number of coating cycles up to three, results in an increase of the Ru loading (up to 8.1 mg_{Ru} g^{-1} instead of 1.4 mg_{Ru} g^{-1}). A further increase in the number of cycles however, did not result in a further enhanced Ru loading. Thus, a silica nanofibrous veil coated with a 2 g L^{-1} Ru@MIL-101 solution at a speed of 170 mm min^{-1} for 3 cycles was chosen as catalysts for the Sabatier reaction. To remove the particles that were only loosely attached to the support, a sample with this optimized coating was flushed with pressurized air for 15 s, later on denoted as brushing treatment. This resulted in a 25% decrease of the Ru loading (Table 1), but is expected to result in a more durable catalyst.

3.3. Ru-catalyzed CO_2 methanation

The synthesized Ru@MIL-101 @Silica nanofibrous veil was evaluated for the CO_2 methanation reaction using a tubular reactor in which the CH_4 formation was analyzed as a function of time, as described in Section 2.7. The specific activity of the nanofibrous veil was determined and compared to the activity of the pure Ru@MIL-101 nanoparticles at 200 °C. For completeness, an overview of the activity of the pure Ru@MIL-101 at all temperatures is given in Fig. S4 of the Supporting Information. For this, the Ru contents determined with ICP-OES (Table 1) were used. For both the Ru@MIL-101 nanoparticles and the functionalized nanofibrous veil, the specific activity at 200 °C amounts to 0.09 $mmol_{CH4}$ $g_{Ru}^{-1}s^{-1}$ (see Fig. 6). With this, it is showcased that applying the Ru@MIL-101 nanoparticles onto silica nanofibrous membranes as macroscopic carrier material preserves the catalytic performance of Ru for the Sabatier reaction.

An in-depth investigation of this new stand-alone catalytic material was performed by varying the reaction temperature (namely 200, 225, 250 and 300 °C), and analyzing the CO_2 conversion, long-term stability and the resulting apparent turnover frequency. These temperatures were chosen to optimize both the conversion and selectivity, allowing the optimal balance between the conflicting kinetic and thermodynamic effects. More specifically, low conversion rates ensure that the actual intrinsic specific activity is measured (far enough from the thermodynamic equilibrium), and low operating temperatures allow high CH_4 selectivity. In all cases, a CH_4 selectivity above 99% was achieved. As expected, the catalytic activity increases significantly upon increasing the temperature, see Fig. 6. Optimal determination of the activity, and thus also the apparent turnover frequency, is established in the low CO_2 conversion regime [99]. Because all experiments in Fig. 6 were measured with the same reactor loading, and thus resulting in a different total Ru loading for the catalytic nanofibrous veils compared to the Ru@ -MIL101 particles on their own, the CO_2 conversion increases upon increasing the temperature (see Fig. S5 in the Supporting Information). Therefore, the measured specific activity is slightly lower than the expected exponential Arrhenius increase upon increasing the reaction temperature (as exemplified in Fig. S4 in the Supporting Information).

Further investigation of the potential of the silica nanofibrous veils as macroscopic carrier of nano-scale catalysts was conducted by performing an introductory stability test for 48 h at 225 °C, see Fig. 7. For completeness, a comparison of the Ru@MIL-101 @Silica nanofibrous veils with and without a brushing treatment is reported. The non-treated catalyst showcases a progressive decrease of the activity in time, which

Table 1
Overview of the Ru content per gram sample determined using IPC-OES of the functionalized MIL-101 nanoparticles, and the resulting dip-coated silica nanofibrous structures before and after catalytic testing. To enhance the long-term stability, an air brushing treatment was applied prior to catalysis. The Ru content after the 48 h stability tests are also established with ICP-OES.

Type of material	Ru Content Pre catalysis (mg g^{-1} sample)	Ru content Post catalysis of 48 h (mg g^{-1} sample)
Ru@MIL-101	113	–
Ru@MIL-101 @Silica nanofibrous veil – 1 x coated	1.4 ± 0.5	–
Ru@MIL-101 @Silica nanofibrous veil – 2 x coated	3.0 ± 0.4	–
Ru@MIL-101 @Silica nanofibrous veil – 3 x coated	8.1 ± 1.3	3.5
Ru@MIL-101 @Silica nanofibrous veil – 3 x coated + brushing treatment	6.3	4.6

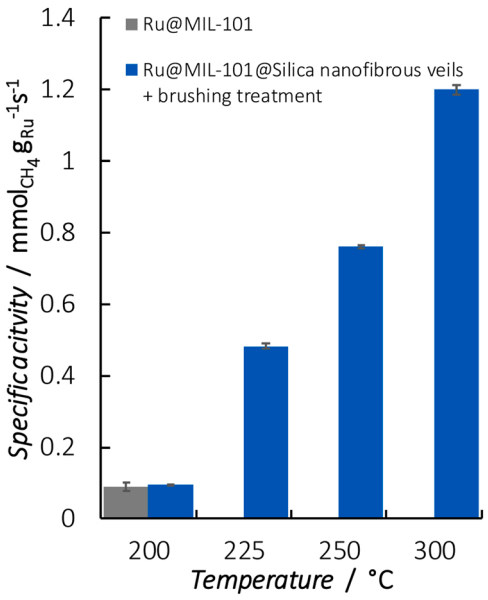

Fig. 6. CO_2 methanation activities of the Ru@MIL-101 @Silica nanofibrous veils with a brushing treatment as a function of the reaction temperature (blue) and of the Ru@MIL-101 powder at 200 °C as comparison (gray). It is showcased that the catalytic veil possesses high potential as macroscopic catalytic material.

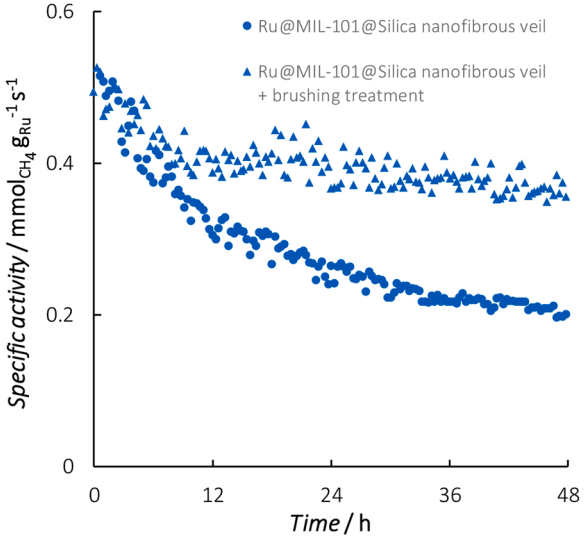

Fig. 7. Long-term stability measurements of the Ru@MIL-101 @Silica nanofibrous veils with and without brushing treatment at 225 °C (expressed as the evolution of the specific activity in time), proving the relevance of the brushing treatment to allow a stable macro-catalyst.

is readily circumvented using the airbrushing treatment. This resulted in a lower initial Ru content in the Ru@MIL-101 @Silica nanofibrous veil (Table 1), but in a significant increase in the stability of the catalytic fibers (Fig. 7). However, more prolonged durability studies on an optimized pilot scale setup are required in future work to support these data [100]. Based on the Ru content after catalytic testing, it can be noted that handling, cutting and loading of the nanofibrous veils in the reactor resulted in a decrease of the amount of Ru. This points to some of the Ru@MIL-101 particles tending to detach from the veils. This was confirmed by SEM images of the silica nanofibers before and after the catalytic experiments, which show that the small particles remain on the fibers and a lower number of larger clusters are observed (see Fig. S6 in the Supporting Information). Upon applying the brushing treatment, the adhesion of the remaining nanoparticles on the fibers is improved.

Hydrogen chemisorption experiments were conducted to have an estimation of the amount of accessible Ru atoms in both the Ru@MIL-101 and the air-brushed functionalized silica nanofibrous catalysts. The previously given Ru contents, measured through ICP-OES, give the total Ru present in the material, whereas H_2 chemisorption provides the amount of Ru that is accessible for H_2. The Ru nanoparticles embedded in the MIL-101 cages have a nanoparticle size of 2–3 nm, resulting in a theoretical dispersion slightly above 20%. Accordingly, a reaction rate can be calculated based on the total amount of Ru, and an apparent turnover frequency (TOF) can be calculated based on the surface accessible Ru (Table 2), since the number of active sites in heterogeneous catalysis is not directly defined. In the latter case, this is still an 'apparent TOF' since not all Ru surface atoms will be actual active sites. Optimal determination of the TOF is obtained when the conversion rate in the reactor is low. Combined with the optimal temperature to level out the opposite kinetic and thermodynamic effects of the Sabatier reaction [101], the TOF at 200 °C was established for both the nanofibrous and powder catalyst. A reaction rate based on the total amount of Ru of 32 and 34 h^{-1} for the Ru@MIL-101 and Ru@MIL-101 @Silica nanofibrous veils was obtained respectively. The Ru@MIL-101 has a 11.3 wt % Ru loading, of which 9% is available at the surface for H_2. This results in an apparent TOF of 358 ± 46 h^{-1} at 200 °C. For the Ru@MIL-101 @Silica nanofibrous veils, 8.5% of the Ru is surface accessible. This corresponds to an apparent TOF of 404 ± 6 h^{-1} at 200 °C (based on surface accessible Ru). In case of the catalytic membranes, the conversion in the used reactor remained below 30% till 250 °C, as a result of the lower amount of Ru in the reactor (0.63 mg vs. 3.39 mg). Therefore, the TOF at elevated temperatures is worthwhile reporting (Table 2), namely the apparent TOF at 250 °C of the Ru@MIL-101 @Silica nanofibrous veil is as high as 3257 ± 19 h^{-1}. For completeness, the measured reaction rate and TOF at 300 °C is also provided (see italic line in Table 2), but due to the high CO_2 conversion the actual TOF will be higher.

This results in a catalyst with a TOF in the same order of magnitude and competitive with the state-of-the-art heterogeneous nanoscale catalyst for the Sabatier reaction [14,19,22,101–107]. An overview of some other catalysts investigated for the Sabatier reaction is given in Table 3. As compared to the results obtained by Kim et al. on a highly active Ru/TiO_2 (rutile) catalysts [22], using the same experimental set-up and conditions, we observe that the TOF is very similar (216 h^{-1} vs. 404 h^{-1} for the catalytic veils). Another study on a Ru/Al_2O_3 catalyst was also carried out in similar conditions, reaching a TOF of 4720 h^{-1} at 280 °C (vs. 3257 h^{-1} for the catalytic veils, at 250 °C). A broader comparison with other systems reported in the literature is difficult because the reaction conditions (gas composition, temperature, pressure, contact time) differ significantly over the various studies [14]. Further, many studies focus on the maximal CO_2 conversion, which means that no reliable values of intrinsic specific activity or TOF can be determined. From Table 3, however, it is evident that the specific activity and TOF values obtained with the new catalytic veils presented here compare well with values that are typically reported with more classical (powdery) catalysts. It is important to note that the proof-of-concept testing described in this work does make use of a reactor designed for powder materials, and is thus not adapted for the specific membrane structure. This however still results in a competitive catalyst, proving the large potential of this catalyst.

Development of a membrane reactor for the Sabatier reaction are of interest in the process intensification logic because membrane reactors are multifunctional reactors, since they combine the possibility for reaction and separation steps in the same apparatus [23,108,109]. In addition, having a macroscopic and easy-to-handle catalytic material at our disposal with a large available surface area and tunable Ru loading based on non-sintering Ru nanoparticles, constitutes a decisive advantage towards the design of an efficient high throughput CO_2 methanation process compared to the catalytic nanoparticles on their own.

Also note that the use of the silica nanofibrous carrier avoids the need for pellet formation of the Ru@MIL-101 nanoparticles, which is required for the use of nanoscale catalysts on an industrial level. In this way, a significant decrease of the TOF, as a result of the decrease in surface area and thus dispersion of the Ru [22]. Additionally, the Ru modified nanofibers possess the important practical advantage of easy handling and recovery. Moreover, using this catalyst design in a reactor compared to pellets generally results in a lower pressure drop of the feed stream [115], making this catalytic composite material the ideal candidate for further investigation in the process intensification of the Sabatier reaction. Ultimately, it is showcased that investigation into the use of inorganic catalytic nanofibrous carriers, which showcase a high thermal and chemical resistance, in membrane reactors is a very promising route to allow process intensification.

4. Conclusion

The use of Ru nanoparticles encapsulated in MIL-101 MOF structures, distributed onto silica nanofibrous veils has been studied as structured heterogeneous catalyst for the Sabatier reaction. An efficient catalyst is obtained by using a two-step Ru-encapsulation method to obtain Ru@MIL-101 particles. Silica nanofibrous membranes prepared by direct electrospinning were used as carrier of the Ru@MIL-101 nanoparticles to obtain a catalytic material that is easy to handle. By dip-coating of the nanofibers in an ethanolic suspension of Ru@MIL-101 (3 consecutive coatings at 170 mm min^{-1} in a 2 g L^{-1} solution), a homogenous distribution of the particles was obtained, without loss in

Table 2
Comparison of the apparent turnover frequencies for the Ru@MIL-101 nanoparticles and the Ru@MIL-101 @Silica nanofibrous catalyst for the Sabatier reaction.

Catalyst	Amount of Ru in reactor (mg)	Catalyst dispersion (%)	T (°C)	CO_2 conversion (%)	Reaction rate – based on total Ru content[a] (h^{-1})	TOF – based on H_2 accessible Ru[b] (h^{-1})
Ru@MIL-101	3.39	9	200	19	32 ± 4	358 ± 46
Ru@MIL-101 @Silica nanofibrous veil + brushing treatment	0.63	8.5	200	3.2	34 ± 1	404 ± 6
			225	16	175 ± 2	2064 ± 29
			250	26	277 ± 1	3257 ± 19
			300	*40*	*436 ± 5*[c]	*5134 ± 59*[c]

[a] Determined with ICP-OES analysis after catalytic testing.
[b] Determined with H_2 chemisorption analysis.
[c] Underestimated because calculated at too high conversion level.

Table 3
Overview of Ru-based CO_2 methanation catalysts reported in literature.

Catalyst	H_2:CO_2 (v/v%)	T (°C)	CO_2 conversion (%)	CH_4 selectivity (%)	TOF[a] (h^{-1})	Ref.
Ru/TiO_2	4:1	150	0	0	0	[110]
		200	15	68	290	
		250	40	78	770	
		300	70	85	1350	
RuO_2/TiO_2	4:1	200	0	0	0	
		250	25	75	450	
		300	50	85	900	
Ru/TiO_2	4:1	200	37	> 99	216	[22]
$Ru/\gamma\text{-}Al_2O_3$	4:1	280	< 1	> 99	4720	[111]
$Ru/Ce_{0.9}Cr_{0.1}O_x$	4:1	225	5	> 99	224	[112]
		250	70	> 99	540	
Ru/TiO_2	3:1	200	1	> 99	15	[36]
		250	3	> 99	45	
		300	8–20	> 99	119–298	
Ru/MnO_x	4:1	300	25	90	180	[33]
Ru/Al_2O_3	4:1	300	32	94	1368	
Ru/CeO_2	4:1	300	83	99	540	
Ru/ZnO	4:1	300	1	6	14.4	
Ru/CeO_2	4:1	450	55	99	–	[113]
Ru/CeO_2	4:1	150	< 10	99	2.2 ± 0.1	[114]
		200	35	> 99	–	[24]
		250	90	> 99	–	
		300	93	–	–	
$Ru/\alpha\text{-}Al_2O_3$	4:1	200	0	–	–	[24]
		250	5	> 99	2.5 ± 0.2	
		300	55	–	–	
Ru/TiO_2	80.9:15.5	350	60	> 99	83	[37]

[a] Based on total Ru content.

porosity of the membrane and large cluster formation of the nanoparticles.

Both the Ru@MIL-101 nanoparticles and the Ru modified silica nanofibrous veils were active in the hydrogenation of CO_2 to CH_4, with an apparent TOF as high as 358 h^{-1} and 404 h^{-1} (based on the surface accessible Ru) at 200 °C for the Ru@MIL-101 nanoparticles and for the Ru@MIL-101 @Silica nanofibrous veil respectively. The apparent TOF reached 3257 h^{-1} at 250 °C for the catalytic veil, for which an air brushing step was introduced to remove the loosely bound nanoparticles from the fiber matrix and ensure a better on-stream stability. Therefore, the use of silica nanofibrous structures as macroscopic carrier for the Ru@MIL-101 is proven to be an attractive alternative for nanoscale powder-based catalysts due to the significant advantages of being easy to handle, recover and reuse, and the low pressure requirements of the gas feed. Thus, this system, namely inorganic nanofibrous membranes as catalytic carrier, paves the way towards membrane reactors and research into process intensification of inorganic nanofibrous membranes as highly thermal and chemical resistant catalytic carrier in a broad range of applications.

CRediT authorship contribution statement

Eva Loccufier: Investigation, Visualization, Writing – original draft, Writing – review & editing, Conceptualization, Validation, Data curation, Project administration. **Geert Watson:** Investigation, Visualization, Writing – original draft, Data curation. **Yingrui Zhao:** Investigation, Data curation, Resources. **Maria Meledina:** Investigation, Data curation, Resources. **Robbe Denis:** Data curation, Investigation. **Parviz Gohari Derakhshandeh:** Conceptualization, Resources. **Pascal Van Der Voort:** Writing – original draft, Conceptualization, Supervision. **Karen Leus:** Writing – original draft, Conceptualization, Data curation, Supervision. **Damien P. Debecker:** Writing – original draft, Writing – review & editing, Conceptualization, Supervision. **Klaartje De Buysser:** Writing – original draft, Conceptualization, Supervision. **Karen De Clerck:** Writing – original draft, Writing – review & editing, Conceptualization, Supervision.

Declaration of Competing Interest

The authors declare that they have no known competing financial interests or personal relationships that could have appeared to influence the work reported in this paper.

Data availability

Data will be made available on request.

Acknowledgments

The Research Foundation – Flanders (FWO) is gratefully acknowledged by E.L. for funding the research through a SB Ph.D. grant (1S82920N). PGD gratefully acknowledge the financial support from the Research Foundation Flanders grant No. G000117N. K.D.C. thanks BOF-UGent (BAS funding and BOF project 2019). M.M. wants to acknowledge the Verbundvorhaben iNEW: Inkubator Nachhaltige Elektrochemische Wertschöpfungsketten with the funding number 03SF0589A (German Federal Ministry for Economic Affairs and Energy BMWi) for financial support. The authors acknowledge the funding from the European Union's Horizon 2020 research and innovation program under grant agreement no. 823717-ESTEEM3. Paulina Melo Bravo is thanked for performing preliminary catalytic tests on the veils. Chidharth Krishnaraj is thanked for performing preliminary chemisorption experiments. Damien P. Debecker thanks the Francqui Foundation for the Francqui Research Professor chair.

Appendix A. Supporting information

Supplementary data associated with this article can be found in the online version at doi:10.1016/j.apcatb.2022.121972.

References

[1] D. Tilman, M. Clark, D.R. Williams, K. Kimmel, S. Polasky, C. Packer, Future threats to biodiversity and pathways to their prevention, Nature 546 (2017) 73, https://doi.org/10.1038/nature22900.

[2] C. Mora, D. Spirandelli, E.C. Franklin, J. Lynham, M.B. Kantar, W. Miles, C. Z. Smith, K. Freel, J. Moy, L.V. Louis, E.W. Barba, K. Bettinger, A.G. Frazier, J. F. Colburn IX, N. Hanasaki, E. Hawkins, Y. Hirabayashi, W. Knorr, C.M. Little, K. Emanuel, J. Sheffield, J.A. Patz, C.L. Hunter, Broad threat to humanity from cumulative climate hazards intensified by greenhouse gas emissions, Nat. Clim. Chang. 8 (2018) 1062–1071, https://doi.org/10.1038/s41558-018-0315-6.

[3] M. Springmann, D.M. Croz, S. Robinson, T. Garnett, H.C.J. Godfray, D. Gollin, M. Rayner, P. Ballon, Global and regional health effects of future food production under climate change: a modelling study, Lancet 387 (2016) 1937–1946, https://doi.org/10.1016/S0140-6736(15)01156-3.

[4] P. Lahijani, Z. Alimuddin, M. Mohammadi, A. Rahman, Conversion of the greenhouse gas CO_2 to the fuel gas CO via the Boudouard reaction: a review, Renew. Sustain. Energy Rev. 41 (2015) 615–632, https://doi.org/10.1016/j.rser.2014.08.034.

[5] C. Song, Global challenges and strategies for control, conversion and utilization of CO_2 for sustainable development involving energy, catalysis, adsorption and chemical processing, Catal. Today 115 (2006) 2–32, https://doi.org/10.1016/j.cattod.2006.02.029.

[6] Y. Zheng, W. Zhang, Y. Li, J. Chen, B. Yu, J. Wang, L. Zhang, Energy related CO_2 conversion and utilization: advanced materials/nanomaterials, reaction mechanisms and technologies, Nano Energy 40 (2017) 512–539, https://doi.org/10.1016/j.nanoen.2017.08.049.

[7] E. Alper, O.Y. Orhan, CO_2 utilization: developments in conversion processes, Petroleum 3 (2017) 109–126, https://doi.org/10.1016/j.petlm.2016.11.003.

[8] S. Bhattacharyya, K.C. Jayachandrababu, Y. Chiang, D.S. Sholl, S. Nair, Butanol separation from humid CO_2-containing multicomponent vapor mixtures by zeolitic imidazolate frameworks, ACS Sustain. Chem. Eng. 5 (2017) 9467–9476, https://doi.org/10.1021/acssuschemeng.7b02604.

[9] L.C. Buelens, V.V. Galvita, H. Poelman, C. Detavernier, G.B. Marin, Super-dry reforming of methane intensifies CO_2 utilization via le Chatelier's principle, Science 354 (80-) (2016) 449–452, https://doi.org/10.1126/science.aah7161.

[10] P. Melo Bravo, D.P. Debecker, Combining CO_2 capture and catalytic conversion to methane, Waste Dispos. Sustain. Energy 1 (2019) 53–65, https://doi.org/10.1007/s42768-019-00004-0.

[11] A. Pustovarenko, A. Dikhtiarenko, A. Bavykina, L. Gevers, A. Ramírez, A. Russkikh, S. Telalovic, A. Aguilar, J.L. Hazemann, S. Ould-Chikh, J. Gascon, Metal-organic framework-derived synthesis of cobalt indium catalysts for the hydrogenation of CO_2 to methanol, ACS Catal. 10 (2020) 5064–5076, https://doi.org/10.1021/acscatal.0c00449.

[12] D. Uysal, Equilibrium analyses and kinetics of carbon dioxide methanation using an alumina-supported ruthenium catalyst, Chem. Eng. Technol. 44 (2021) 1939–1946, https://doi.org/10.1002/ceat.202100146.

[13] S. Escorihuela, C. Cerdá-Moreno, F. Weigelt, S. Remiro-Buenamañana, S. Escolástico, A. Tena, S. Shishatskiy, T. Brinkmann, A. Chica, J.M. Serra, Intensification of catalytic CO_2 methanation mediated by in-situ water removal through a high-temperature polymeric thin-film composite membrane, J. CO_2 Util. 55 (2022), 101813, https://doi.org/10.1016/J.JCOU.2021.101813.

[14] J. Ashok, S. Pati, P. Hongmanorom, Z. Tianxi, C. Junmei, S. Kawi, A review of recent catalyst advances in CO_2 methanation processes, Catal. Today (2020), https://doi.org/10.1016/j.cattod.2020.07.023.

[15] L. Guerra, S. Rossi, J. Rodrigues, J. Gomes, J. Puna, M.T. Santos, Methane production by a combined Sabatier reaction/water electrolysis process, J. Environ. Chem. Eng. 6 (2018) 671–676, https://doi.org/10.1016/j.jece.2017.12.066.

[16] A. Sternberg, A. Bardow, Life cycle assessment of power-to-gas: syngas vs methane, ACS Sustain. Chem. Eng. 4 (2016) 4156–4165, https://doi.org/10.1021/acssuschemeng.6b00644.

[17] G. Leonzio, Process analysis of biological Sabatier reaction for bio-methane production, Chem. Eng. J. 290 (2016) 490–498, https://doi.org/10.1016/j.cej.2016.01.068.

[18] C. Vogt, M. Monai, G.J. Kramer, B.M. Weckhuysen, The renaissance of the Sabatier reaction and its applications on Earth and in space, Nat. Catal. 2 (2019) 188–197, https://doi.org/10.1038/s41929-019-0244-4.

[19] T. Abe, M. Tanizawa, K. Watanabe, A. Taguchi, CO_2 methanation property of Ru nanoparticle-loaded TiO2 prepared by a polygonal barrel-sputtering method, Energy Environ. Sci. 2 (2009) 315–321, https://doi.org/10.1039/b817740f.

[20] W. Li, X. Nie, X. Jiang, A. Zhang, F. Ding, M. Liu, Z. Liu, X. Guo, C. Song, ZrO2 support imparts superior activity and stability of Co catalysts for CO_2 methanation, Appl. Catal. B Environ. 220 (2018) 397–408, https://doi.org/10.1016/J.APCATB.2017.08.048.

[21] A. Kim, C. Sanchez, B. Haye, C. Boissière, C. Sassoye, D.P. Debecker, Mesoporous TiO2 support materials for Ru-based CO_2 methanation catalysts, ACS Appl. Nano Mater. 2 (2019) 3220–3230, https://doi.org/10.1021/acsanm.9b00518.

[22] A. Kim, D.P. Debecker, F. Devred, V. Dubois, C. Sanchez, C. Sassoye, CO_2 methanation on Ru/TiO2 catalysts: On the effect of mixing anatase and rutile TiO2 supports, Appl. Catal. B Environ. 220 (2018) 615–625, https://doi.org/10.1016/j.apcatb.2017.08.058.

[23] P. Bernardo, A. Iulianelli, F. Macedonio, E. Drioli, Membrane technologies for space engineering, J. Membr. Sci. 626 (2021), 119177, https://doi.org/10.1016/j.memsci.2021.119177.

[24] F. Wang, S. He, H. Chen, B. Wang, L. Zheng, M. Wei, D.G. Evans, X. Duan, Active site dependent reaction mechanism over Ru/CeO2 catalyst toward CO_2 methanation, J. Am. Chem. Soc. 138 (2016) 6298–6305, https://doi.org/10.1021/jacs.6b02762.

[25] M. Schubert, S. Pokhrel, A. Thomé, V. Zielasek, T.M. Gesing, F. Roessner, L. Mädler, M. Bäumer, Highly active Co-Al2O3-based catalysts for CO_2 methanation with very low platinum promotion prepared by double flame spray pyrolysis, Catal. Sci. Technol. 6 (2016) 7449–7460, https://doi.org/10.1039/c6cy01252c.

[26] S. Li, Y. Xu, Y. Chen, W. Li, L. Lin, M. Li, Y. Deng, X. Wang, B. Ge, C. Yang, S. Yao, J. Xie, Y. Li, X. Liu, D. Ma, Tuning the selectivity of catalytic carbon dioxide hydrogenation over iridium/cerium oxide catalysts with a strong metal–support interaction, Angew. Chem. Int. Ed. 56 (2017) 10761–10765, https://doi.org/10.1002/anie.201705002.

[27] A. Beuls, C. Swalus, M. Jacquemin, G. Heyen, A. Karelovic, P. Ruiz, Methanation of CO_2: further insight into the mechanism over Rh/γ-Al2O3 catalyst, Appl. Catal. B Environ. 113–114 (2012) 2–10, https://doi.org/10.1016/J.APCATB.2011.02.033.

[28] G. Zhou, H. Liu, K. Cui, A. Jia, G. Hu, Z. Jiao, Y. Liu, X. Zhang, Role of surface Ni and Ce species of Ni/CeO2 catalyst in CO_2 methanation, Appl. Surf. Sci. 383 (2016) 248–252, https://doi.org/10.1016/J.APSUSC.2016.04.180.

[29] D.C.D. da Silva, S. Letichevsky, L.E.P. Borges, L.G. Appel, The Ni/ZrO2 catalyst and the methanation of CO and CO_2, Int. J. Hydrog. Energy 37 (2012) 8923–8928, https://doi.org/10.1016/J.IJHYDENE.2012.03.020.

[30] G. Zhou, T. Wu, H. Xie, X. Zheng, Effects of structure on the carbon dioxide methanation performance of Co-based catalysts, Int. J. Hydrog. Energy 38 (2013) 10012–10018, https://doi.org/10.1016/J.IJHYDENE.2013.05.130.

[31] R. Razzaq, C. Li, M. Usman, K. Suzuki, S. Zhang, A highly active and stable Co4N/γ-Al2O3 catalyst for CO and CO_2 methanation to produce synthetic natural gas (SNG), Chem. Eng. J. 262 (2015) 1090–1098, https://doi.org/10.1016/J.CEJ.2014.10.073.

[32] I. Kuznecova, J. Gusca, Property based ranking of CO and CO 2 methanation catalysts, Energy Procedia 128 (2017) 255–260, https://doi.org/10.1016/j.egypro.2017.09.068.

[33] J.A.H. Dreyer, P. Li, L. Zhang, G.K. Beh, R. Zhang, P.H.-L. Sit, W.Y. Teoh, Influence of the oxide support reducibility on the CO_2 methanation over Ru-based catalysts, Appl. Catal. B Environ. 219 (2017) 715–726, https://doi.org/10.1016/J.APCATB.2017.08.011.

[34] S. López-Rodríguez, A. Davó-Quiñonero, E. Bailón-García, D. Lozano-Castelló, A. Bueno-López, Effect of Ru loading on Ru/CeO2 catalysts for CO_2 methanation, Mol. Catal. 515 (2021), https://doi.org/10.1016/j.mcat.2021.111911.

[35] H.T.T. Nguyen, Y. Kumabe, S. Ueda, K. Kan, M. Ohtani, K. Kobiro, Highly durable Ru catalysts supported on CeO2 nanocomposites for CO_2 methanation, Appl. Catal. A Gen. 577 (2019) 35–43, https://doi.org/10.1016/J.APCATA.2019.03.011.

[36] Z. Zhao, Q. Jiang, Q. Wang, M. Wang, J. Zuo, H. Chen, Q. Kuang, Z. Xie, Effect of rutile content on the catalytic performance of Ru/TiO2 catalyst for low-temperature CO_2 methanation, ACS Sustain. Chem. Eng. 9 (2021) 14288–14296, https://doi.org/10.1021/acssuschemeng.1c05565.

[37] A.M. Abdel-Mageed, K. Wiese, M. Parlinska-Wojtan, J. Rabeah, A. Brückner, R. J. Behm, Encapsulation of Ru nanoparticles: modifying the reactivity toward CO and CO_2 methanation on highly active Ru/TiO2 catalysts, Appl. Catal. B Environ. 270 (2020), 118846, https://doi.org/10.1016/J.APCATB.2020.118846.

[38] P. Chowdhury, C. Bikkina, S. Gumma, Gas adsorption properties of the chromium-based metal organic framework MIL-101, J. Phys. Chem. C 113 (2009) 6616–6621.

[39] L. Hamon, C. Serre, T. Devic, T. Loiseau, F. Millange, Comparative study of hydrogen sulfide adsorption in the MIL-53 (Al, Cr, Fe), MIL-47 (V), MIL-100 (Cr), and MIL-101 (Cr) metal-organic frameworks at room temperature, J. Am. Chem. Soc. 53 (2009) 8775–8777.

[40] P.L. Llewellyn, S. Bourrelly, C. Serre, A. Vimont, M. Daturi, L. Hamon, G. De Weireld, J. Chang, D. Hong, Y.K. Hwang, S.H. Jhung, High uptakes of CO_2 and CH4 in mesoporous metals organic frameworks MIL-100 and MIL-101, Langmuir (2008) 7245–7250.

[41] Z. Zhang, S. Huang, S. Xian, H. Xi, Z. Li, Adsorption equilibrium and kinetics of CO_2 on chromium terephthalate MIL-101, Energy Fuels (2011) 835–842, https://doi.org/10.1021/ef101548g.

[42] K. Munusamy, G. Sethia, D.V. Patil, P.B. Somayajulu Rallapalli, R.S. Somani, H. C. Bajaj, Sorption of carbon dioxide, methane, nitrogen and carbon monoxide on MIL-101(Cr): Volumetric measurements and dynamic adsorption studies, Chem. Eng. J. 195–196 (2012) 359–368, https://doi.org/10.1016/J.CEJ.2012.04.071.

[43] G. Liu, V. Chernikova, Y. Liu, K. Zhang, Y. Belmabkhout, O. Shekhah, C. Zhang, S. Yi, M. Eddaoudi, W.J. Koros, Mixed matrix formulations with MOF molecular sieving for key energy-intensive separations, Nat. Mater. 17 (2018) 283–289, https://doi.org/10.1038/s41563-017-0013-1.

[44] S. Ma, D. Sun, X. Wang, H. Zhou, A mesh-adjustable molecular sieve for general use in gas separation, Angew. Chem. Int. Ed. (2007) 2458–2462, https://doi.org/10.1002/anie.200604353.

[45] R. Kitaura, K. Seki, G. Akiyama, S. Kitagawa, Porous coordination-polymer crystals with gated channels specific for supercritical gases, Angew. Chem. Int. Ed. 42 (2003) 428–431.

[46] J. Fu, S. Das, G. Xing, T. Ben, V. Valtchev, S. Qiu, Fabrication of COF-MOF composite membranes and their highly selective separation of $H2/CO_2$, J. Am. Chem. Soc. 138 (2016) 7673–7680, https://doi.org/10.1021/jacs.6b03348.

[47] J. Lee, O.K. Farha, J. Roberts, K.A. Scheidt, S.T. Nguyen, J.T. Hupp, Metal–organic framework materials as catalysts, Chem. Soc. Rev. 38 (2009) 1450–1459, https://doi.org/10.1039/b807080f.

[48] K. Shen, X. Chen, J. Chen, Y. Li, Development of MOF-derived carbon-based nanomaterials for efficient catalysis, ACS Catal. 6 (2016) 5887–5903, https://doi.org/10.1021/acscatal.6b01222.

[49] F.N. Al-rowaili, A. Jamal, M.S.B. Shammakh, A. Rana, A review on recent advances for electrochemical reduction of carbon dioxide to methanol using

metal–organic framework (MOF) and non-MOF catalysts: challenges and future prospects, ACS Sustain. Chem. Eng. 6 (2018) 15895–15914, https://doi.org/10.1021/acssuschemeng.8b03843.
[50] M. Meledina, G. Watson, A. Meledin, P. Van Der Voort, J. Mayer, K. Leus, Ru catalyst encapsulated into the pores of mil-101 mof: Direct visualization by tem, Materials 14 (2021), https://doi.org/10.3390/ma14164531.
[51] N. Cao, T. Liu, J. Su, X. Wu, W. Luo, G. Cheng, Ruthenium supported on MIL-101 as an efficient catalyst for hydrogen generation from hydrolysis of amine boranes, New J. Chem. 38 (2014) 4032–4035, https://doi.org/10.1039/C4NJ00739E.
[52] B. Sosna, O. Korup, R. Horn, Probing local diffusion and reaction in a porous catalyst pellet, J. Catal. 381 (2020) 285–294, https://doi.org/10.1016/j.jcat.2019.11.005.
[53] S. Whitaker, Mass transport and reaction in catalyst pellets, Transp. Porous Media 2 (1987) 269–299, https://doi.org/10.1007/BF00165785.
[54] B. Kreitz, G.D. Wehinger, T. Turek, Dynamic simulation of the CO_2 methanation in a micro-structured fixed-bed reactor, Chem. Eng. Sci. 195 (2019) 541–552, https://doi.org/10.1016/j.ces.2018.09.053.
[55] A. Porta, L. Falbo, C.G. Visconti, L. Lietti, C. Bassano, P. Deiana, Synthesis of Ru-based catalysts for CO_2 methanation and experimental assessment of intraporous transport limitations, Catal. Today 343 (2020) 38–47, https://doi.org/10.1016/j.cattod.2019.01.042.
[56] T. Granato, F. Testa, R. Olivo, Catalytic activity of HKUST-1 coated on ceramic foam, Microporous Mesoporous Mater. 153 (2012) 236–246, https://doi.org/10.1016/J.MICROMESO.2011.12.055.
[57] Z.G. Gu, W.Q. Fu, X. Wu, J. Zhang, Liquid-phase epitaxial growth of a homochiral MOF thin film on poly(l-DOPA) functionalized substrate for improved enantiomer separation, Chem. Commun. 52 (2016) 772–775, https://doi.org/10.1039/c5cc07614e.
[58] K. Leus, C. Krishnaraj, L. Verhoeven, V. Cremers, J. Dendooven, R. K. Ramachandran, P. Dubruel, P. Van Der Voort, Catalytic carpets: Pt@MIL-101@ electrospun PCL, a surprisingly active and robust hydrogenation catalyst, J. Catal. 360 (2018) 81–88, https://doi.org/10.1016/j.jcat.2018.01.018.
[59] A. Ricca, L. Truda, V. Palma, Study of the role of chemical support and structured carrier on the CO_2 methanation reaction, Chem. Eng. J. 377 (2019), 120461, https://doi.org/10.1016/J.CEJ.2018.11.159.
[60] M. Coto, S.C. Troughton, J. Duan, R.V. Kumar, T.W. Clyne, Development and assessment of photo-catalytic membranes for water purification using solar radiation, Appl. Surf. Sci. 433 (2018) 101–107, https://doi.org/10.1016/j.apsusc.2017.10.027.
[61] H. Song, J. Shao, J. Wang, X. Zhong, The removal of natural organic matter with LiCl-TiO2-doped PVDF membranes by integration of ultrafiltration with photocatalysis, Desalination 344 (2014) 412–421, https://doi.org/10.1016/j.desal.2014.04.012.
[62] M. Gutiérrez-Arzaluz, L. Noreña-Franco, S. Ángel-Cuevas, V. Mugica-Álvarez, M. Torres-Rodríguez, Catalysts with cerium in a membrane reactor for the removal of formaldehyde pollutant from water effluents, Molecules 21 (2016), https://doi.org/10.3390/molecules21060668.
[63] I.F.J. Vankelecom, Polymeric membranes in catalytic reactors, Chem. Rev. 102 (2002) 3779–3810, https://doi.org/10.1021/cr0103468.
[64] O. Iglesias, M.J. Rivero, A.M. Urtiaga, I. Ortiz, Membrane-based photocatalytic systems for process intensification, Chem. Eng. J. 305 (2016) 136–148, https://doi.org/10.1016/j.cej.2016.01.047.
[65] E. Drioli, A.I. Stankiewicz, F. Macedonio, Membrane engineering in process intensification-an overview, J. Membr. Sci. 380 (2011) 1–8, https://doi.org/10.1016/j.memsci.2011.06.043.
[66] A. Helmi, E. Fernandez, J. Melendez, D.A.P. Tanaka, F. Gallucci, M. Van Sint Annaland, Fluidized bed membrane reactors for ultra pure H2 production - a step forward towards commercialization, Molecules 21 (2016), https://doi.org/10.3390/molecules21030376.
[67] J. Coronas, J. Santamaría, Catalytic reactors based on porous ceramic membranes, Catal. Today 51 (1999) 377–389, https://doi.org/10.1016/S0920-5861(99)00090-5.
[68] X. Dong, W. Jin, N. Xu, K. Li, Dense ceramic catalytic membranes and membrane reactors for energy and environmental applications, Chem. Commun. 47 (2011) 10886–10902, https://doi.org/10.1039/c1cc13001c.
[69] T. Mayer-Gall, J.W. Lee, K. Opwis, B. List, J.S. Gutmann, Textile catalysts - an unconventional approach towards heterogeneous catalysis, ChemCatChem 8 (2016) 1428–1436, https://doi.org/10.1002/cctc.201501252.
[70] J. Kubota, T. Okumura, Methane synthesis from CO_2 and H2O with electricity using H-permeable membrane electrochemical cells with Ru catalyst and phosphate electrolyte, Sustain. Energy Fuels 5 (2021) 935–940, https://doi.org/10.1039/D0SE01896A.
[71] F. Dalena, A. Senatore, M. Basile, S. Knani, A. Basile, A. Iulianelli, Advances in methanol production and utilization, with particular emphasis toward hydrogen generation via membrane reactor technology, Membranes 8 (2018), https://doi.org/10.3390/membranes8040098.
[72] A. Catarina Faria, C.V. Miguel, A.E. Rodrigues, L.M. Madeira, Modeling and simulation of a steam-selective membrane reactor for enhanced CO_2 methanation, Ind. Eng. Chem. Res. 59 (2020) 16170–16184, https://doi.org/10.1021/acs.iecr.0c02860.
[73] Z. Liu, Z. Bian, Z. Wang, B. Jiang, A CFD study on the performance of CO_2 methanation in a water-permeable membrane reactor system, React. Chem. Eng. 7 (2022) 450–459, https://doi.org/10.1039/D1RE00401H.
[74] M.M. Alinejad, K. Ghasemzadeh, A. Iulianelli, S. Liguori, M. Ghahremani, CFD development of a silica membrane reactor during HI decomposition reaction coupling with CO_2 methanation at sulfur-iodine cycle, Nanomaterials 12 (2022), https://doi.org/10.3390/nano12050824.
[75] Z. Li, Y. Deng, N. Dewangan, J. Hu, Z. Wang, X. Tan, S. Liu, S. Kawi, High temperature water permeable membrane reactors for CO_2 utilization, Chem. Eng. J. 420 (2021), 129834, https://doi.org/10.1016/j.cej.2021.129834.
[76] S. Homaeigohar, Y. Davoudpour, Y. Habibi, M. Elbahri, The electrospun ceramic hollow nanofibers, Nanomaterials 7 (2017) 383, https://doi.org/10.3390/nano7110383.
[77] D. Malwal, P. Gopinath, Fabrication and applications of ceramic nanofibers in water remediation: a review, Crit. Rev. Environ. Sci. Technol. 46 (2016) 500–534, https://doi.org/10.1080/10643389.2015.1109913.
[78] H. Esfahani, R. Jose, S. Ramakrishna, Electrospun ceramic nanofiber mats today: synthesis, properties, and applications, Materials 10 (2017), https://doi.org/10.3390/ma10111238.
[79] W. Li, Q. Meng, C. Zhang, G. Zhang, Metal–organic framework/PVDF composite membranes with high H2 permselectivity synthesized by ammoniation, Chem. Eur. J. 21 (2015) 7224–7230, https://doi.org/10.1002/chem.201500007.
[80] L. Eykens, K. De Sitter, C. Dotremont, L. Pinoy, B. Van der Bruggen, Membrane synthesis for membrane distillation: a review, Sep. Purif. Technol. 182 (2017) 36–51, https://doi.org/10.1016/j.seppur.2017.03.035.
[81] T. Chen, Z. Wang, L. Liu, S. Pati, M.H. Wai, S. Kawi, Coupling CO_2 separation with catalytic reverse water-gas shift reaction via ceramic-carbonate dual-phase membrane reactor, Chem. Eng. J. 379 (2020), 122182, https://doi.org/10.1016/J.CEJ.2019.122182.
[82] H.C. Wu, Z. Rui, J.Y.S. Lin, Hydrogen production with carbon dioxide capture by dual-phase ceramic-carbonate membrane reactor via steam reforming of methane, J. Membr. Sci. 598 (2020), 117780, https://doi.org/10.1016/J.MEMSCI.2019.117780.
[83] H. Wu, W. Pan, D. Lin, H. Li, Electrospinning of ceramic nanofibers: fabrication, assembly and applications, J. Adv. Ceram. 1 (2012) 2–23, https://doi.org/10.1007/s40145-012-0002-4.
[84] S. Ramakrishna, R. Jose, P.S. Archana, A.S. Nair, R. Balamurugan, J. Venugopal, W.E. Teo, Science and engineering of electrospun nanofibers for advances in clean energy, water filtration, and regenerative medicine, J. Mater. Sci. 45 (2010) 6283–6312, https://doi.org/10.1007/s10853-010-4509-1.
[85] F.E. Tuler, E.M. Gaigneaux, E.E. Miró, V.G. Milt, D.P. Debecker, Catalytic ceramic papers for diesel soot oxidation: a spray method for enhanced performance, Catal. Commun. 72 (2015) 116–120, https://doi.org/10.1016/j.catcom.2015.09.013.
[86] A. Baji, Y.-W. Mai, Engineering ceramic fiber nanostructures through polymer-mediated electrospinning, in: Z. Lin, Y. Yang, A. Zhang (Eds.), Polymer-Engineered Nanostructures for Advanced Energy Applications, Springer International Publishing, Cham, 2017, pp. 3–30, https://doi.org/10.1007/978-3-319-57003-7_1.
[87] A. Greiner, J.H. Wendorff, Electrospinning: a fascinating method for the preparation of ultrathin fibers, Angew. Chem. Int. Ed. 46 (2007) 5670–5703, https://doi.org/10.1002/anie.200604646.
[88] M. Shahhosseininia, S. Bazgir, M.D. Joupari, Fabrication and investigation of silica nanofibers via electrospinning, Mater. Sci. Eng. C 91 (2018) 502–511, https://doi.org/10.1016/J.MSEC.2018.05.068.
[89] E. Loccufier, J. Geltmeyer, L. Daelemans, D.R. D'hooge, K. De Buysser, K. De Clerck, Silica nanofibrous membranes for the separation of heterogeneous azeotropes, Adv. Funct. Mater. 28 (2018) 1–10, https://doi.org/10.1002/201804138.
[90] J. Geltmeyer, L. Van Der Schueren, F. Goethals, K. De Buysser, K. De Clerck, Optimum sol viscosity for stable electrospinning of silica nanofibres, J. Sol-Gel Sci. Technol. 67 (2013) 188–195, https://doi.org/10.1007/s10971-013-3066-x.
[91] J. Geltmeyer, J. De Roo, F. Van den Broeck, J.C. Martins, K. De Buysser, K. De Clerck, The influence of tetraethoxysilane sol preparation on the electrospinning of silica nanofibers, J. Sol-Gel Sci. Technol. 77 (2016) 453–462, https://doi.org/10.1007/s10971-015-3875-1.
[92] S.-S. Choi, S.G. Lee, S.S. Im, S.H. Kim, Y.L. Joo, Silica nanofibers from eletrospinning/sol-gel process, J. Mater. Sci. Lett. 22 (2003) 891–893, https://doi.org/10.1023/A.
[93] K. Leus, T. Bogaerts, J. De Decker, H. Depauw, K. Hendrickx, H. Vrielinck, V. Van Speybroeck, P. Van Der Voort, Systematic study of the chemical and hydrothermal stability of selected "stable" metal organic frameworks, Microporous Mesoporous Mater. 226 (2016) 110–116, https://doi.org/10.1016/j.micromeso.2015.11.055.
[94] M. Ding, X. Cai, H.L. Jiang, Improving MOF stability: approaches and applications, Chem. Sci. 10 (2019) 10209–10230, https://doi.org/10.1039/c9sc03916c.
[95] R. Fang, H. Liu, R. Luque, Y. Li, Efficient and selective hydrogenation of biomass-derived furfural to cyclopentanone using Ru catalysts, Green Chem. 17 (2015) 4183–4188, https://doi.org/10.1039/c5gc01462j.
[96] J. Geltmeyer, J. De Roo, F. Van den Broeck, J.C. Martins, K. De Buysser, K. De Clerck, The influence of tetraethoxysilane sol preparation on the electrospinning of silica nanofibers, J. Sol-Gel Sci. Technol. 77 (2016) 453–462, https://doi.org/10.1007/s10971-015-3875-1.
[97] E. Loccufier, J. Geltmeyer, L. Daelemans, D.R. D'hooge, K. De Buysser, K. De Clerck, Silica nanofibrous membranes for the separation of heterogeneous azeotropes, Adv. Funct. Mater. 28 (2018), https://doi.org/10.1002/adfm.201804138.
[98] A. Kovács, R. Schierholz, K. Tillmann, FEI Titan G2 80-200 CREWLEY, J. Large-Scale Res. Facil. JLSRF 2 (2016) 68–71, https://doi.org/10.17815/jlsrf-2-68.

[99] E. Moioli, N. Gallandat, A. Züttel, Model based determination of the optimal reactor concept for Sabatier reaction in small-scale applications over Ru/Al2O3, Chem. Eng. J. 375 (2019), 121954, https://doi.org/10.1016/j.cej.2019.121954.
[100] E. Moioli, N. Gallandat, A. Züttel, Parametric sensitivity in the Sabatier reaction over Ru/Al2O3-theoretical determination of the minimal requirements for reactor activation, React. Chem. Eng. 4 (2019) 100–111, https://doi.org/10.1039/c8re00133b.
[101] E. Moioli, A. Züttel, A model-based comparison of Ru and Ni catalysts for the Sabatier reaction, Sustain. Energy Fuels 4 (2020) 1396–1408, https://doi.org/10.1039/C9SE00787C.
[102] A. Kim, C. Sanchez, G. Patriarche, O. Ersen, S. Moldovan, A. Wisnet, C. Sassoye, D.P. Debecker, Selective CO_2 methanation on Ru/TiO2 catalysts: unravelling the decisive role of the TiO2 support crystal structure, Catal. Sci. Technol. 2 (2016) 8117–8128, https://doi.org/10.1039/c6cy01677d.
[103] W.J. Lee, C. Li, H. Prajitno, J. Yoo, J. Patel, Y. Yang, S. Lim, Recent trend in thermal catalytic low temperature CO_2 methanation: a critical review, Catal. Today (2020), https://doi.org/10.1016/j.cattod.2020.02.017.
[104] P.J. Lunde, F.L. Kester, Rates of methane formation from carbon dioxide and hydrogen over a ruthenium catalyst, J. Catal. 30 (1973) 423–429, https://doi.org/10.1016/0021-9517(73)90159-0.
[105] P. Panagiotopoulou, D.I. Kondarides, X.E. Verykios, Selective methanation of CO over supported noble metal catalysts: effects of the nature of the metallic phase on catalytic performance, Appl. Catal. A Gen. 344 (2008) 45–54, https://doi.org/10.1016/j.apcata.2008.03.039.
[106] G. Du, S. Lim, Y. Yang, C. Wang, L. Pfefferle, G.L. Haller, Methanation of carbon dioxide on Ni-incorporated MCM-41 catalysts: the influence of catalyst pretreatment and study of steady-state reaction, J. Catal. 249 (2007) 370–379, https://doi.org/10.1016/j.jcat.2007.03.029.
[107] A. Petala, P. Panagiotopoulou, Methanation of CO_2 over alkali-promoted Ru/TiO2 catalysts: I. Effect of alkali additives on catalytic activity and selectivity, Appl. Catal. B Environ. 224 (2018) 919–927, https://doi.org/10.1016/j.apcatb.2017.11.048.
[108] H. Ohya, J. Fun, H. Kawamura, K. Itoh, H. Ohashi, M. Aihara, S. Tanisho, Y. Negishi, Methanation of carbon dioxide by using membrane reactor integrated with water vapor permselective membrane and its analysis, J. Membr. Sci. 131 (1997) 237–247, https://doi.org/10.1016/S0376-7388(97)00055-0.
[109] H.T. Hwang, A. Harale, P.K.T. Liu, M. Sahimi, T.T. Tsotsis, A membrane-based reactive separation system for CO_2 removal in a life support system, J. Membr. Sci. 315 (2008) 116–124, https://doi.org/10.1016/J.MEMSCI.2008.02.018.
[110] Y. Li, Z. Liu, Z. Rao, F. Yu, W. Bao, Y. Tang, H. Zhao, J. Zhang, Z. Wang, J. Li, Z. Huang, Y. Zhou, Y. Li, B. Dai, Experimental and theoretical insights into an enhanced CO 2 methanation mechanism over a Ru-based catalyst, Appl. Catal. B Environ. 319 (2022), 121903, https://doi.org/10.1016/j.apcatb.2022.121903.
[111] C. Janke, M.S. Duyar, M. Hoskins, R. Farrauto, Catalytic and adsorption studies for the hydrogenation of CO_2 to methane, Appl. Catal. B Environ. 152–153 (2014) 184–191, https://doi.org/10.1016/J.APCATB.2014.01.016.
[112] X. Xu, L. Liu, Y. Tong, X. Fang, J. Xu, D.E. Jiang, X. Wang, Facile Cr3+-doping strategy dramatically promoting Ru/CeO2 for low-temperature CO_2 methanation: unraveling the roles of surface oxygen vacancies and hydroxyl groups, ACS Catal. 11 (2021) 5762–5775, https://doi.org/10.1021/acscatal.0c05468.
[113] S. Sharma, Z. Hu, P. Zhang, E.W. McFarland, H. Metiu, CO_2 methanation on Ru-doped ceria, J. Catal. 278 (2011) 297–309, https://doi.org/10.1016/j.jcat.2010.12.015.
[114] F. Wang, C. Li, X. Zhang, M. Wei, D.G. Evans, X. Duan, Catalytic behavior of supported Ru nanoparticles on the {100}, {110}, and {111} facet of CeO2, J. Catal. 329 (2015) 177–186, https://doi.org/10.1016/j.jcat.2015.05.014.
[115] A. Basile, M. De Falco, G. Centi, G. Iaquaniello, Membrane Reactor Engineering: Applications for a Greener Process Industry, Wiley, 2016. ⟨https://books.google.be/books?id=g6PkDAAAQBAJ⟩.